JOM, Vol. 66, No. 10, 2014
DOI: 10.1007/s11837-014-1059-z
© 2014 The Minerals, Metals & Materials Society

Phase Stability of Low-Density, Multiprincipal Component Alloys Containing Aluminum, Magnesium, and Lithium

X. YANG,[1] S.Y. CHEN,[1] J.D. COTTON,[2,3] and Y. ZHANG[1,4]

1.—High-Entropy Theory Center, State Key Laboratory for Advanced Metals and Materials, University of Science and Technology Beijing, Beijing 100083, China. 2.—Metallic Materials Group, The Boeing Company, MC 19-HP, PO Box 3707, Seattle, WA 98124-2207, USA. 3.—e-mail: james.d.cotton@boeing.com. 4.—e-mail: drzhangy@ustb.edu.cn

A series of low-density, multiprincipal component alloys containing high concentrations of Al, Mg, Li, Zn, Cu and/or Sn was designed using a strategy based on high-entropy alloys (HEAs). The alloys were prepared by induction melting under high-purity argon atmosphere, and the resulting microstructures were characterized in the as-cast condition. The resulting microstructures are multiphase and complex and contain significant volume fractions of disordered solutions and intermetallic compounds. By analyzing the atomic size difference, enthalpy of mixing, entropy of mixing, electronegativity difference, and valence electron concentration among the constituent elements, modified phase formation rules are developed for low-density multiprincipal component alloys that are more restrictive than previously established limits based on more frequently studied HEAs comprising mostly transition metals. It is concluded that disordered solid solution phases are generally less stable than competing ordered compounds when formulated from low-density elements including Al, Mg, and Li.

INTRODUCTION

Over the past decade, a new class of multiprincipal component alloys, often referred to as high-entropy alloys (HEAs), has attracted attention from many research groups across the world owing to their complex microstructures and promising properties, and a considerable number of such systems has been investigated for both functional and structural applications.[1–6] These alloys may be defined as containing multiple (nominally ≥5) principle elements, and each element has an atomic percentage between 5% and 35%.[7,8] According to Boltzmann's hypothesis based on the regular solution model, HEAs may exhibit a relatively high entropy of mixing in liquid state or regular solution state.[1,9–11] Therefore, when cooling from the molten state, HEAs are intended to form simple, disordered, hexagonal close-packed (HCP), face-centered cubic (FCC), and/or body-centered cubic (BCC) solid solutions rather than ordered phases, which may be expected in terms of known binary phase equilibria. In practice, the total number of observed phases is often below the maximum equilibrium number allowed by the Gibbs phase rule. If achieved, such microstructures can be expected to exhibit high strength via high order solution hardening, fine scale constituents due to reduced characteristic diffusion lengths, and considerable opportunity for microstructural design. Furthermore, the availability of a large number of constituent elements and phases opens the door to unusual and tailored chemical, corrosion, and oxidation behaviors.[4,10,12–16] Thus, HEAs may be viewed as an evolutionary step in the development of structural and functional metallic materials systems.

Most HEA research to date has focused on steel-like alloys for industrial applications. The well-studied HEA systems usually contain the transition metal elements, such as Cr, Mn, Fe, Co, Ni, Zr, Ti, and Cu, often destabilized with modest amounts of Al. It is conceivable that some of these multiprincipal component alloys will compete with high-performance steels and stainless steels. In addition, American researchers have recently explored refractory metal HEAs for high-temperature applications, which are composed of later transition metal elements such as Ta, W, Nb, Mo, V, Hf,

(Published online July 22, 2014)

and Ti. The resulting refractory metal HEAs appear to possess competitive mechanical properties and good thermal stability.[17–19] However, the raw material cost, difficulty in melting, and especially, high density of such HEAs systems are prohibitive to structural aerospace and airframe components, except in cases where high-temperature strength is a major design driver (e.g., aeropropulsion hardware).

In contrast to HEAs, common structural alloys in the aviation industry are based on a single principal element, such as, Al, Ti, Fe, or Ni, with other minor elements contained as alloying additions for modifying microstructure and properties.[20–24] Despite steady improvements in performance, the evolutionary approach for designing and optimizing lightweight alloy compositions has limits and will need to be superseded by new approaches to materials design. For these reasons, a HEA strategy was evaluated in an attempt to identify new, low-density metallic materials systems that may be considered for the aviation industry.

To this end, we have investigated a series of low-density multicomponent alloys based on the Al-Li-Mg-(Zn, Cu, Sn) system, which were designed according to a published high-entropy alloying strategy.[6] Two variants with a higher Al content, $Al_{80}Li_5Mg_5Zn_5Sn_5$ and $Al_{80}Li_5Mg_5Zn_5Cu_5$, were also evaluated to explore the lower density design space. Microstructures, phase compositions, and mechanical behaviors are described herein.

EXPERIMENTAL PROCEDURES

The selected alloying elements and corresponding alloy design parameters[25,26] are listed in Table I, and target chemical compositions corresponding to AlLiMgZnSn, $AlLi_{0.5}MgZn_{0.5}Sn_{0.2}$, $AlLi_{0.5}MgZn_{0.5}Cu_{0.2}$, $AlLi_{0.5}MgCu_{0.5}Sn_{0.2}$, $Al_{80}Li_5Mg_5Zn_5Sn_5$, and $Al_{80}Li_5Mg_5Zn_5Cu_5$ were fabricated.

Small laboratory ingots were prepared by induction melting a mixture of high-purity metals with the purity better than 99.5 weight percent (wt.%) under high-purity argon atmosphere in a graphite crucible. Because of lithium's high reactivity in air, a master alloy of Al-Li containing 27 wt.% Li was substituted. To achieve a homogeneous distribution of elements, each alloy ingot was melted multiple times to achieve a total of 30 min in the liquid state. Each such prepared alloy button was then suction cast into a steel mold under high vacuum (5×10^{-3} Pa) to obtain cylindrical rods of 45–55 mm in diameter and length of about 120 mm.

The microstructure and properties of each alloy were studied in the as-cast condition. Crystal structures were characterized by x-ray diffraction (XRD) using a PHILIPS APD-10 diffractometer with Cu Kα radiation using samples in the form of about 2-mm-thick plates. Microstructures were examined using a ZEISS SUPRA 55 scanning electron microscope (SEM) with energy-dispersive spectrometry (EDS). The specimens for microstructure observation were ground, polished, and then etched with Keller's reagent. Cylindrical samples with the form of 3 mm diameter $\times$ 6 mm (aspect ratio of 2) were electric-discharged machined from each cast alloy ingot for compression tests by using an MTS 809 load frame at room temperature with a strain rate of 5×10^{-4} s^{-1}. The density of each alloy was measured by the Archimedes method.

RESULTS

Density

The theoretical densities (ρ_{theor}) of these alloys were estimated using a rule of mixtures assumption of a disordered solid solution and listed in Table II, as given by:[19]

$$\rho_{\text{theor}} = \frac{\sum_{i=1}^{n} c_i A_i}{\sum_{i=1}^{n} c_i A_i / \rho_i} \quad (1)$$

where, c_i, A_i, and ρ_i are the weight fraction, atomic weight, and density of each ith respective constituent element, and n is the total number of elements.

The densities measured by the Archimedes method for these alloys (ρ_{exp}) are listed in Table II. The measured density for most chemistries deviated significantly from the corresponding theoretical density, suggesting that ordered phases are present.

Table I. Atomic radius (r), standard atomic weight (A), crystal structure, electronegativity (χ), value electron concentration (VEC), density (ρ), and melting temperature (T_m) for constituent elements in present alloys

Alloy Design Elements	Al	Li	Mg	Zn	Cu	Sn
r (10^{-10} m)	1.43	1.56	1.60	1.39	1.28	1.55
A (g/mol)	26.98	6.94	24.31	65.39	63.55	118.7
Crystal structure	FCC	BCC	HCP	HCP	FCC	Tetragonal
χ	1.61	0.98	1.31	1.65	1.90	1.96
VEC	3	1	2	12	11	4
ρ (g/cm^3)	2.70	0.54	1.74	7.13	8.93	7.37
T_m (K)	933.5	453.7	922	692.7	1358	505.1

Table II. Theoretical (ρ_{theor}) and measured densities (ρ_{exp}), and chemical compositions (at.%) of phases identified in the microstructures of AlLiMgZnSn, $AlLi_{0.5}MgZn_{0.5}Sn_{0.2}$, $AlLi_{0.5}MgZn_{0.5}Cu_{0.2}$, $AlLi_{0.5}MgCu_{0.5}Sn_{0.2}$, $Al_{80}Li_5Mg_5Zn_5Sn_5$, and $Al_{80}Li_5Mg_5Zn_5Cu_5$ alloys

Alloys	ρ_{theor} (g/cm^3)	ρ_{exp} (g/cm^3)	Regions	Measured chemical composition (at.%) Al	Mg	Zn	Sn	Cu
AlLiMgZnSn	3.88	4.23	A	0	62.8	1.79	35.41	–
			B	54.65	0	44.59	0.76	–
			C	89.44	0	10.56	0	–
			D	0	0	11.31	88.69	–
$AlLi_{0.5}MgZn_{0.5}Sn_{0.2}$	2.98	3.22	A	36.25	35.51	28.23	0	–
			B	0	58.93	3.02	38.04	–
			C	83.45	12.75	3.79	0	–
$AlLi_{0.5}MgZn_{0.5}Cu_{0.2}$	2.96	3.73	A	39.26	37.79	16.34	–	6.61
			B	32.87	32.46	15.70	–	18.97
			C	70.36	20.12	8.77	–	0.74
$AlLi_{0.5}MgCu_{0.5}Sn_{0.2}$	3.45	3.69	A	49.05	34.06	–	0	16.88
			B	36.76	35.09	–	0	28.15
			C	4.30	22.12	–	73.58	0
$Al_{80}Li_5Mg_5Zn_5Sn_5$	2.84	3.05	A	87.83	1.47	3.89	6.81	–
			B	8.20	2.47	3.95	85.38	–
$Al_{80}Li_5Mg_5Zn_5Cu_5$	2.87	3.08	A	94.54	1.88	2.38	–	1.20
			B	72.23	0	1.87	–	25.91

Phase Constituents and Microstructures

The XRD patterns of each alloy are given in Fig. 1. All majority phases are identified; for clarity, unknown phases are not indicated. Corresponding secondary electron images are shown in Fig. 2. The microstructures are generally complex, with typically at least three constituents observed in each alloy, and notable differences between the different alloys. The compositions of the constituents, as measured by EDS analysis, are listed in Table II. Note that Li is not included in the analyses due to inadequate EDS peak intensity.

The XRD pattern of the specimens of equiatomic AlLiMgZnSn alloy is shown in Fig. 1a. The phase makeup is significantly more complex compared with previously published HEAs that usually contain only FCC and/or BCC phases. The reflections of ordered Mg_2Sn and/or Li_2MgSn phases are observed on the diffraction pattern of these alloys, in addition to the terminal α-Al, α-Zn, and α-Sn based solid solution phases. However, 2θ angles of the diffraction peaks for Mg_2Sn are very close to that for Li_2MgSn, thus, suggesting a probable isomorph or solubility extension of the same phase. Taking into account that the intensities of the diffraction peaks of ordered phases are frequently stronger than those of solid solution phases, the volume fractions of intermetallic phases appear to predominate. The microstructure of equiatomic AlLiMgZnSn alloy is presented in Fig. 2a. At least four constituents (marked by A, B, C, and D, respectively) with different contrasts can be seen in the SEM image. The magnified SEM secondary electron image of region B is shown in the inset of Fig. 2a; a mixture of the fine white network phase and black matrix phase is observed in this region. When combined with the EDS analysis results listed in Table II, the phase constituents of different regions in the AlLiMgZnSn equiatomic alloy can be identified. Region A (matrix) appears to be Mg_2Sn, while region B is a mixture of α-Al + α-Zn solutions, region C (dark precipitate) is α-Al and region D (light precipitate) is a Sn-rich solid solution. A minor second phase can also be seen in region A, which can be identified as the Li_2MgSn phase that exists in the Mg-Li-Sn ternary. Since the aluminum content is below the eutectoid composition of the equilibrium Al-Zn binary phase diagram, one may conclude that the mixture in region B represents a hypoeutectoid structure, and the primary phase is the α-Al FCC solid solution. It is also useful to note the fine solidification cracks in the Mg_2Sn phase, suggesting that this intermetallic compound phase is relatively brittle.

For the $AlLi_{0.5}MgZn_{0.5}Sn_{0.2}$ alloy, the Li, Zn, and Sn contents are decreased relative to the equiatomic alloy. The corresponding XRD pattern shown in Fig. 1b identifies at least three phases, $Mg_{32}(AlZn)_{49}$, Mg_2Sn or Li_2MgSn, and the FCC Al-rich solid solution. Figure 2b shows the microstructure of $AlLi_{0.5}MgZn_{0.5}Sn_{0.2}$ alloy, with three different constituents (marked by A, B, and C, respectively) identified, which is consistent with the XRD analysis results. According to the SEM and EDS results (listed in Table II), it may be concluded that the regions A (matrix), B (light precipitate), and C (dark precipitate) correspond to the $Mg_{32}(AlZn)_{49}$, Mg_2Sn, and α-Al solid solution phases, respectively. Fine cracks are also observed in Mg_2Sn phase as above.

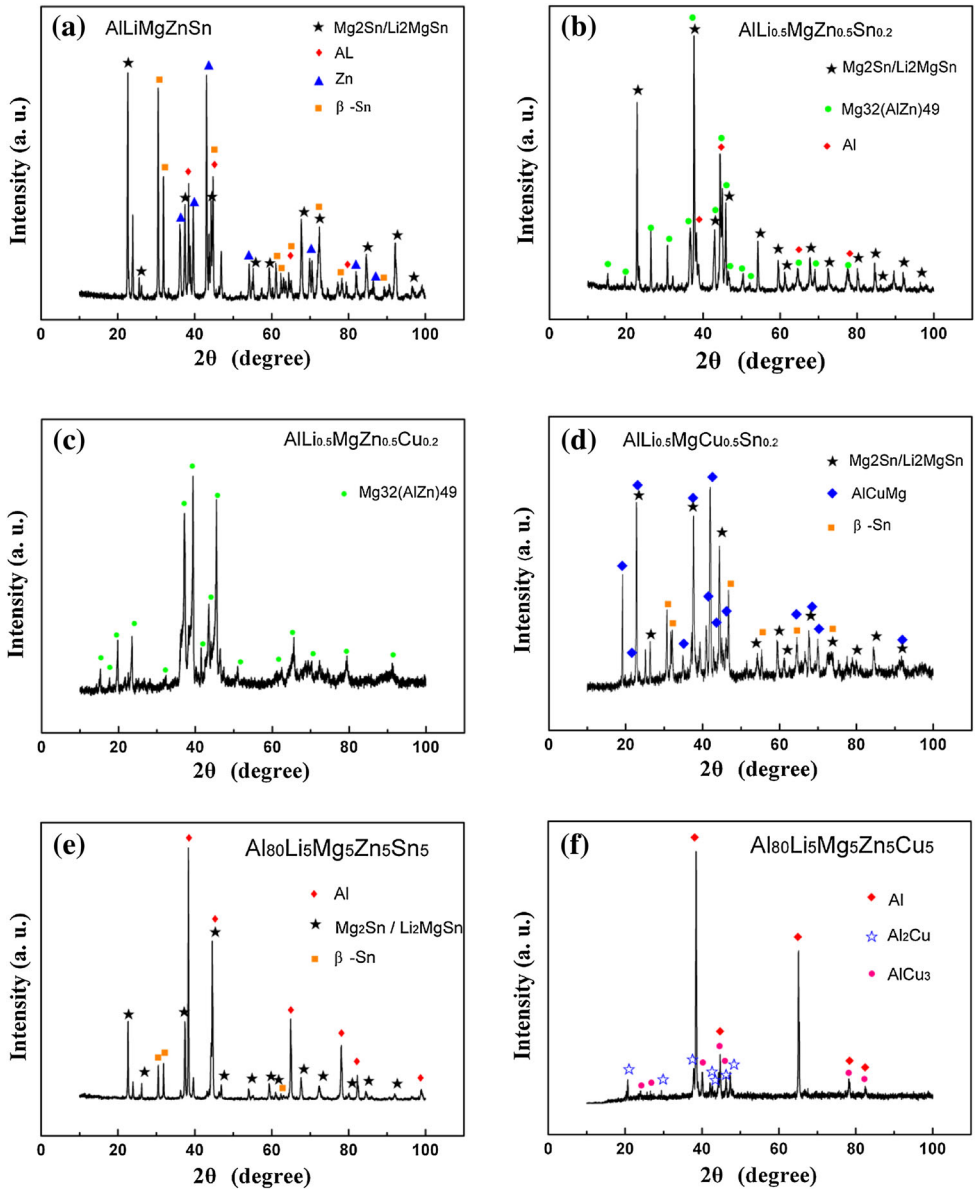

Fig. 1. XRD patterns of low-density multicomponent alloys. (a) AlLiMgZnSn; (b) $AlLi_{0.5}MgZn_{0.5}Sn_{0.2}$; (c) $AlLi_{0.5}MgZn_{0.5}Cu_{0.2}$; (d) $AlLi_{0.5}MgCu_{0.5}Sn_{0.2}$; (e) $Al_{80}Li_5Mg_5Zn_5Sn_5$; and (f) $Al_{80}Li_5Mg_5Zn_5Cu_5$ alloys.

When Sn is substituted by Cu in the Al-$Li_{0.5}MgZn_{0.5}Cu_{0.2}$ alloy, only the strong diffraction peaks of the intermetallic phase $Mg_{32}(AlZn)_{47}$ can be identified in the XRD patterns in Fig. 1c. The minor peaks are difficult to index. However, three distinct alloy constituents, marked by A, B, and C, are visible in Fig. 2c. Constituents A and the surrounding region B appear to be the major alloy constituents due to their larger volume fraction in the alloy microstructure. The EDS measurements shows that the contents of Al, Mg, Zn are close to the composition of the $Mg_{32}(AlZn)_{49}$ phase in region A and B, while region B is enriched in Cu. This suggests that regions A and B contain two variants of the ordered $Mg_{32}(AlZn)_{47}$ phase structure, and the composition segregates during solidification, perhaps due to the higher melting temperature of Cu. Region C is enriched in Al and Mg and depleted of Zn and Cu (Table II). Although Li content cannot be measured by EDS, it may be concluded that region C contains mainly Li-rich phase since Li-rich phases occur within the Al-Li-Mg ternary system.

The XRD pattern of the $AlLi_{0.5}MgCu_{0.5}Sn_{0.2}$ alloy sample is shown in Fig. 1d. Diffraction peaks corresponding to AlMgCu phase, α-Sn solid solution phase, and Mg_2Sn or Li_2MgSn phase are observed. According to the SEM image of the microstructure shown in Fig. 2d and the corresponding EDS analysis results listed in Table II, two dominant matrix phases are identified: A, and the constituent of darker contrast, B, may be the AlMgCu phase; lighter phases (marked by C) embedded in the

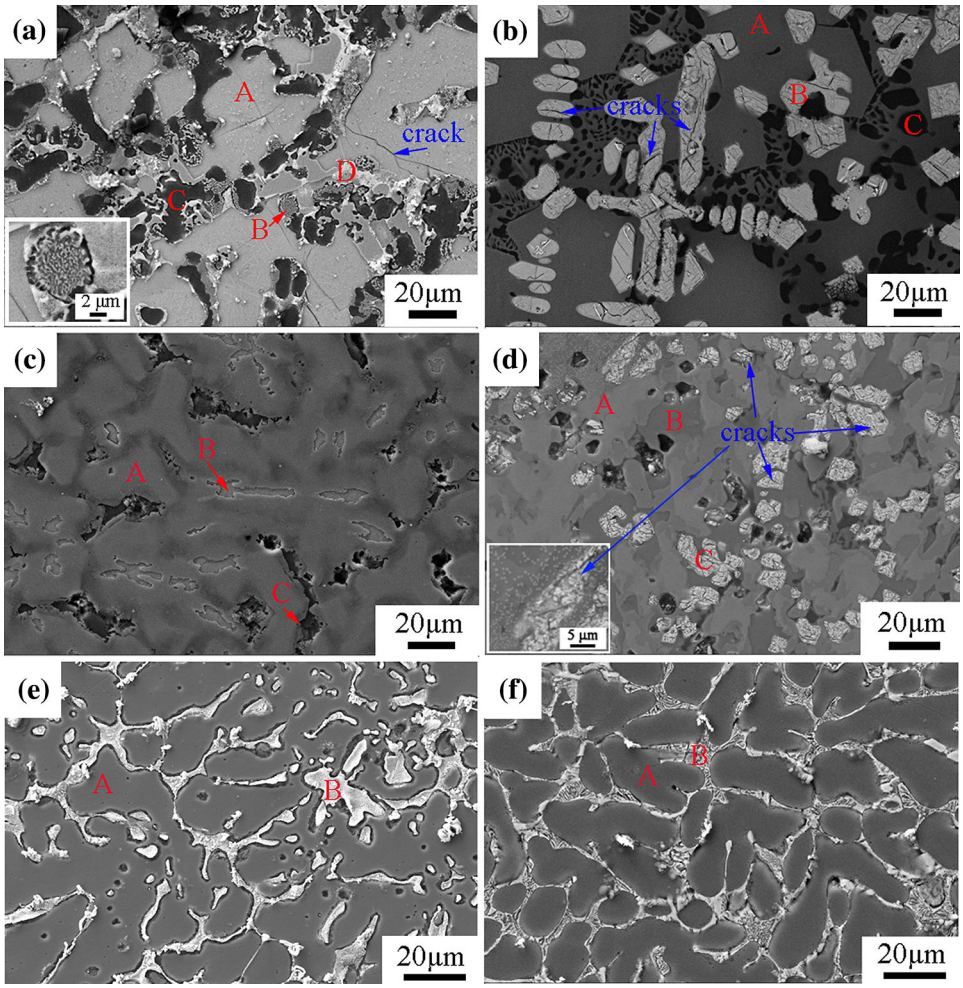

Fig. 2. SEM secondary electron images of low-density multicomponent alloys. (a) AlLiMgZnSn; (b) $AlLi_{0.5}MgZn_{0.5}Sn_{0.2}$; (c) $AlLi_{0.5}MgZn_{0.5}Cu_{0.2}$; (d) $AlLi_{0.5}MgCu_{0.5}Sn_{0.2}$; (e) $Al_{80}Li_5Mg_5Zn_5Sn_5$; and (f) $Al_{80}Li_5Mg_5Zn_5Cu_5$ alloys.

matrix with dark internal precipitates are apparently Sn-rich solid solution phases. Due to the higher melting temperature of Cu and the positive enthalpy between Cu and Sn (shown in Table III), composition segregation is likely to be present within the AlMgCu phase.

The inset in Fig. 2d shows many fine particles are inhomogeneously distributed in localized regions of the microstructure, which could be Mg_2Sn or Li_2MgSn phases. Cracks also appear in the white precipitates, suggesting the Sn-rich phase is the more brittle phase.

The XRD patterns of Al-rich $Al_{80}Li_5Mg_5Zn_5Sn_5$ and $Al_{80}Li_5Mg_5Zn_5Cu_5$ compositions are shown in Fig. 1e and f, respectively. In the former, diffraction peaks corresponding to α-Al phase and two intermetallic compound phases, Al_2Cu phase and $AlCu_3$ phase, are observed. The intensity of the diffraction peaks of FCC α-Al phase exceeds that of the other phases, suggesting a predominant volume fraction of α-Al phase. Similarly, $Al_{80}Li_5Mg_5Zn_5Sn_5$ alloy also appears to contain a majority of FCC α-Al phase, besides the Mg_2Sn/Li_2MgSn and the Sn-solid solution phases. The microstructures of $Al_{80}Li_5Mg_5Zn_5Cu_5$ and $Al_{80}Li_5Mg_5Zn_5Sn_5$ alloys are shown in Fig. 1e and f, respectively. Both alloys display a dendritic cast structure, which is divided by the net-like interdendritic structure. According to the EDS results listed in Table II, the dendrites shown in the SEM images are Al-rich, with the Al content in the dendrite cores in both varying roughly from ~88 at.% to 95 at.%. In the $Al_{80}Li_5Mg_5Zn_5Cu_5$ alloy, fine needle-like Al-Cu phases

Table III. Compressive mechanical properties of selected Al-Li-Mg-(Zn, Sn, Cu) alloys

Alloy	$\sigma_{0.2}$ (MPa)	σ_f (MPa)	ε_p (%)
AlLiMgZnSn	600	615	1.2
$AlLi_{0.5}MgZn_{0.5}Sn_{0.2}$	–	546	–
$Al_{80}Li_5Mg_5Zn_5Cu_5$	488	879	17
$Al_{80}Li_5Mg_5Zn_5Sn_5$	415	836	16

$\sigma_{0.2}$, yield strength; σ_f, fracture strength; ε_p, plastic strain.

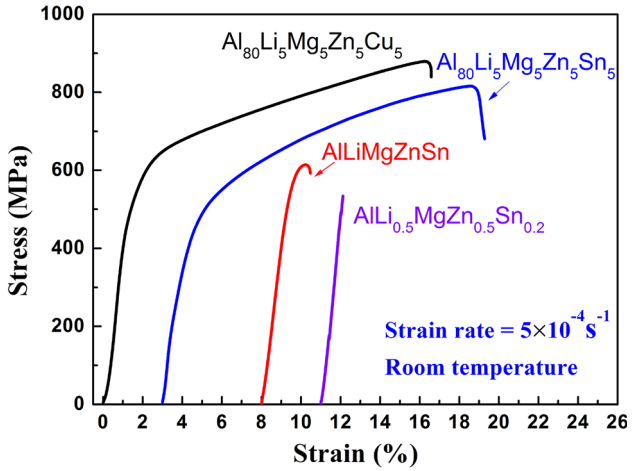

Fig. 3. Compressive engineering stress–strain curves of AlLiMgZnSn, $AlLi_{0.5}MgZn_{0.5}Sn_{0.2}$, $Al_{80}Li_5Mg_5Zn_5Sn_5$, and $Al_{80}Li_5Mg_5Zn_5Cu_5$ alloys at room temperature. The initial strain rate was 5×10^{-4} s^{-1}.

have precipitated in the interdendritic regions, while the interdendritic regions of $Al_{80}Li_5Mg_5Zn_5Sn_5$ alloy are enriched in Sn, Mg_2Sn, or Li_2MgSn phases.

Mechanical Behavior

The room temperature compressive engineering properties for the as-cast AlLiMgZnSn, $AlLi_{0.5}MgZn_{0.5}Sn_{0.2}$, $Al_{80}Li_5Mg_5Zn_5Sn_5$, and $Al_{80}Li_5Mg_5Zn_5Cu_5$ alloys are shown in Table III, and engineering stress strain curves are plotted in Fig. 3. The $AlLi_{0.5}MgZn_{0.5}Cu_{0.2}$ and $AlLi_{0.5}MgCu_{0.5}Sn_{0.2}$ alloys were too brittle to obtain test coupons. All tested alloys exhibited a relatively high strength, with the fracture strength exceeding 500 MPa. However, the AlLiMgZnSn and $AlLi_{0.5}MgZn_{0.5}Sn_{0.2}$ samples failed without visible yielding, and the plastic strain of AlLiMgZnSn alloy reached only about 1.2%. In contrast, the $Al_{80}Li_5Mg_5Zn_5Sn_5$ and $Al_{80}Li_5Mg_5Zn_5Cu_5$ alloys displayed a high yield strength, fracture strength, and compressive strain-to-failure values (17% and 16%, respectively). It is apparent that the plasticity of alloys is improved by compositional shifting to a more Al-rich chemistry that promotes a larger volume fraction of the more ductile α-Al phase.

DISCUSSION

To better understand the phase stability in the present low-density multicomponent alloys, it is valuable to examine the contained binary alloy systems of the constituent elements. Similar consideration has been carried out for CoCrFeMnCu, TiCrFeMnNi, CoMoFeMnNi, CoVFeMnNi, and CoCrVMnNi alloys.[27] Through thermodynamic analyses of the constituent binaries, Otto et al. concluded that the phase stability extended to the higher order quinary alloys. For equiatomic multi-principal element alloy, AlLiMgZnSn, the equilibrium phases for the 10 contained equiatomic binary alloy systems at room temperature are listed in Table IV.[28]

The phases listed in Table IV are stable in the corresponding equiatomic binary alloy system (at the 50/50 equiatomic composition). It is observed that four out of the ten constituent equiatomic binary alloy systems (Al-Li, Al-Mg, Li-Zn, Li-Sn) form single-phase intermetallic compounds at room temperature. In contrast, the Mg-Zn and Mg-Sn equiatomic binary alloy systems consist of one solid solution and one intermetallic compound. In the other four equiatomic binary alloy systems, only disordered solid solution phases form at room temperature, and three of these (Al-Zn, Al-Sn, and Zn-Sn) actually contain two solid solution phases with different crystal structures. Only the Li-Mg system exhibits a single solid solution phase (BCC crystal structure). Thus, the stable phases of the binary alloy systems drive the phase selection in the quinary AlLiMgZnSn alloy, and no new higher order phases are apparent. Of these phases, the high enthalpy contributions for ordered Mg_2Sn phase exceeds the entropy contributions toward stability of the solid solution phases, and becomes the main phase in AlLiMgZnSn alloy in the as-cast condition. For reference, the enthalpies of mixing between the related alloying elements in present alloys are given in Table IV. Despite the predominance of the FCC α-Al solution phase in the $Al_{80}Li_5Mg_5Zn_5Sn_5$ and $Al_{80}Li_5Mg_5Zn_5Cu_5$ alloys, ordered phases have not been avoided.

The present experimental results suggest that the entropic solution effects observed in more "steel-like" CoCrFeNiX multicomponent alloys do not extend to alloys containing elements without a d-orbital. In contrast, ordered phases occurred in all investigated alloys, even in the equiatomic AlLiMgZnSn alloy, which possesses the highest configurational entropy (in the liquid state and metastable single solid solution state) among these alloys (the calculated value of ΔS_{mix} for these alloys is shown in Table V).

The increased entropy of mixing in these alloys is insufficient to restrain compound formation, and other Hume-Rothery type factors control the phase stability and selection in such low-density multicomponent alloys. In fact, it has been shown that while a high entropy of mixing can explain why solid solutions persist in HEAs,[27,29,30] it cannot be used to predict the formation of thermodynamically stabilized solid solutions a priori. To obtain simple solid solution phases in such low-density systems, special phase formation rules for low-density multicomponent alloys must be further evaluated.

In terms of thermodynamics and the Hume-Rothery rules for solid solution formation in binary systems, these other factors include atomic size, enthalpy, electronegativity, and valence electron

Table IV. Equilibrium phases for equiatomic binary systems contained in AlLiMgZnSn alloy at room temperature (in the upper right triangular region) and the values of the enthalpy of mixing, ΔH_{mix} (kJ/mol), calculated by Miedema's model for atomic pairs between the elements used to prepared the low-density multicomponent alloys (in the lower left triangular region)

Element	Al	Li	Mg	Zn	Sn
Al		LiAl	Al_3Mg_2 + $Al_{12}Mg_{17}$	Al (FCC) + Zn (HCP)	Al (FCC) + β-Sn (Tetragonal)
Li	−4		Li (BCC)	LiZn	LiSn
Mg	−2	0		Mg (HCP) + MgZn	Mg_2Sn + β-Sn (Tetragonal)
Zn	1	−7	−4		Zn (HCP) + β-Sn (Tetragonal)
Sn	4	−18	−9	1	
Cu	−1	−5	−3	1	7

concentration. Meanwhile, certain derived parameters, such as δ (atomic size difference), ΔH_{mix} (enthalpy of mixing), Ω (ratio of entropy to enthalpy values), $\Delta\chi$ (Pauling electronegativity difference), and VEC (valence electron concentration), have been developed to characterize phase stability in multicomponent alloys. These are defined as follows:[31–35]

$$\delta = \sqrt{\sum_{i=1}^{n} c_i(1 - r_i/\bar{r})^2} \tag{2}$$

$$\Delta H_{mix} = \sum_{i=1, i\neq j}^{n} \Omega_{ij} c_i c_j \tag{3}$$

$$\Omega = \frac{T_m \Delta S_{mix}}{|\Delta H_{mix}|} \tag{4}$$

$$\Delta\chi = \sqrt{\sum_{i=1}^{n} c_i(\chi_i - \overline{\chi})^2} \tag{5}$$

$$\mathrm{VEC} = \sum_{i=1}^{n} c_i(\mathrm{VEC})_i \tag{6}$$

where c_i or c_j is the atomic percentage of the ith or jth component, $\bar{r}$ is the average atomic radius and r_i is the atomic radius, Ω_{ij} (= $4\Delta H_{AB}^{mix}$) is the regular solution interaction parameter between the ith and jth elements, ΔH_{AB}^{mix} is the enthalpy of mixing of binary liquid alloys, $T_m\left(T_m = \sum_{i=1} n_{c_i}(T_m)_i\right)$ is the melting temperature of n-elements alloy, $(T_m)_i$ is the melting point of the ith component of alloy, $\overline{\chi} = \sum_{i=1}^{n} c_i\chi_i$, χ_i is the Pauling electronegativity for the ith component, and $(\mathrm{VEC})_i$ is the VEC of the ith element.

Among these parameters, atomic size difference, δ, plays a key role in phase selection. A large value of δ may promote either the formation of amorphous phases or ordered intermetallic compounds. Conversely, a small value of δ facilitates the formation of random solid solution and $\delta \leq 6.6\%$ has been suggested as a criterion for forming solid solution phases in multicomponent alloys.[9,32]

The relationships between δ and the other four parameters for representative reported multicomponent HEAs are plotted in Fig. 4.[3,6,9,29,32,34,36] The corresponding alloy compositions and phase constituents derive from reference, and the value of parameters are calculated based on Eqs. 2–6 (for simplicity, details are not included in this paper). Almost all multicomponent HEAs are synthesized by normal arc or induction casting, and some are followed by casting into a copper mold. It is clear that, besides small δ, near-zero values of the absolute ΔH_{mix} (−22 kJ/mol to 5 kJ/mol), large values of Ω ($\sim\geq$1.1) and small $\Delta\chi$ ($\sim\leq$0.175) effectively favor the formation of solid solution rather than that of intermetallic compounds. In other words, $\delta - \Delta H_{mix}$, $\delta - \Omega$, and $\delta - \Delta\chi$ schemes could be used to predict the formation of solid solution phases for multicomponent HEAs. However, as shown in Fig. 4, δ, ΔH_{mix}, Ω, and $\Delta\chi$ are necessary but not sufficient conditions for the formation of solid solution alloys. Some exceptions are apparent in Fig. 4c, for example, for Mo-containing HEAs. Omega (Ω), which combines the effects of entropy of mixing (ΔS_{mix}) and enthalpy of mixing (ΔH_{mix}), has been shown to have a higher accuracy than ΔH_{mix} alone in predicting phase formation for multicomponent alloys, especially for systems with lower calculated configurational entropy. On the other hand, Fig. 4d also shows that VEC can do a reasonable job of predicting the stability of BCC and FCC solid solutions.

The phase selection rules and mapped phase stabilized regions shown in Fig. 4 are based on "traditional" HEAs, which consist of metallic elements containing 3d and/or 4d electron orbitals. One goal of the current investigation was to determine whether constituent elements of low-density HEAs would follow similar rules. To obtain a better understanding of the factors that affect the solid solution phase stability in low-density multicomponent alloys, an additional 11 low-density component alloys (from ternary to quinary) based on the AlLiMg(X,Y) system were fabricated and their compositions and phase constituents evaluated

Table V. Complete list of investigated alloy compositions and calculated values for Ω, Δ, $\Delta\chi$, and VEC

Alloys	Major phases	ΔH_{mix} (kJ/mol)	ΔS_{mix} (J/mol·K)	Ω	δ	$\Delta\chi$	VEC
Initial compositions							
AlLiMgZnSn	$Mg_2Sn/Li_2MgSn + Zn + Al + Sn$	−6.08	13.38	1.56	5.52	0.33	5.40
$AlLi_{0.4}MgZn_{0.5}Sn_{0.2}$	$Mg_2Sn/Li_2MgSn + Mg_{32}(AlZn)_{49} + Al$	−3.61	12.18	2.74	5.63	0.26	5.38
$AlLi_{0.5}MgZn_{0.5}Cu_{0.2}$	$Mg_{32}(AlZn)_{49}$ + Unkown	−3.30	12.31	3.15	6.69	0.26	5.84
$AlLi_{0.5}MgCu_{0.5}Sn_{0.2}$	$AlCuMg + Mg_2Sn/Li_2MgSn + Sn$	−3.65	12.31	3.02	7.58	0.31	5.25
$Al_{80}Li_5Mg_5Zn_5Sn_5$	$Al + Mg_2Sn/Li_2MgSn + Sn$	−0.53	6.47	10.68	3.61	0.15	3.60
$Al_{80}Li_5Mg_5Zn_5Cu_5$	$Al + Al_2Cu + AlCu_3$	−0.61	6.47	9.72	4.09	0.16	3.95
Additional compositions investigated for phase content only							
$(Al_{0.5}Mg_{0.5})_{95}Li_5$	$Al_{12}Mg_{17} + LiMg$ + Unknown phase	−2.2	7.13	2.93	5.48	0.18	4.80
$(Al_{0.5}Mg_{0.5})_{90}Li_{10}$	$Al_{12}Mg_{17} + LiMg$ + Unknown phase	−2.36	7.89	2.94	5.32	0.20	4.60
$(Al_{0.5}Mg_{0.5})_{85}Li_{15}$	$Al_{12}Mg_{17} + LiMg$ + Unknown phase	−2.48	8.41	2.91	5.19	0.23	4.40
$(Al_{0.5}Mg_{0.5})_{75}Li_{25}$	$Al_{12}Mg_{17} + LiMg$ + Unknown phase	−2.64	9.00	2.76	4.89	0.25	4.00
AlMgLi	$Al_{12}Mg_{17} + LiMg$ + Unknown phase	−2.67	9.13	2.63	4.62	0.26	3.67
$Al_{40}Mg_{40}Li_{10}Cu_{10}$	$Al_{12}Mg_{17} + Mg_{32}Al_{47}Cu_7 + AlCuMg$	−2.76	9.92	3.32	7.10	0.25	5.20
$Al_{35}Mg_{35}Li_{15}Cu_{15}$	$Al_{12}Mg_{17} + Mg_{32}Al_{47}Cu_7 + AlCuMg$	−3.08	10.43	2.78	6.82	0.28	5.30
$Al_{40}Mg_{40}Li_{10}Zn_{10}$	$Mg_{32}(AlZn)_{49}$ + HCP	−2.68	9.92	3.17	5.67	0.21	5.30
$Al_{35}Mg_{35}Li_{15}Zn_{15}$	$Mg_{32}(AlZn)_{49}$ + HCP	−3.12	10.43	3.08	5.68	0.23	5.45
$AlLi_{0.5}MgZn_{0.5}Sn_{0.2}$	$Mg_2Sn/Li_2MgSn + Mg_{32}(AlZn)_{49} + Al$	−3.89	12.31	2.50	5.64	0.27	5.41
$Al_{35}Mg_{35}Li_{15}Cu_{10}La_5$	$Al_7CuLa_2 + AlCuMg + Mg_{32}Al_{47}Cu_7 + Al_{12}Mg_{17}$ + Li-rich phase	−6.08	11.64	1.75	8.69	0.42	4.90
$Al_{35}Mg_{35}Li_{15}Cu_{10}Ce_5$	$Al_3CeCu + AlCuMg + Mg_{32}Al_{47}Cu_7 + Al_{12}Mg_{17}$ + Li-rich phase	−6.12	11.64	1.72	8.23	0.42	4.90
$Al_{35}Mg_{35}Li_{15}Zn_{10}La_5$	$Al_2LaZn_2 + Al_{12}Mg_{17}$ + Mg-rich phase	−6.44	11.64	1.53	7.58	0.41	5.00
$Al_{35}Mg_{35}Li_5Zn_{10}Ce_5$	$Al_4Ce + Mg_{32}(AlZn)_{49}$ + Mg-rich phase	−6.52	11.64	1.50	7.03	0.40	5.00

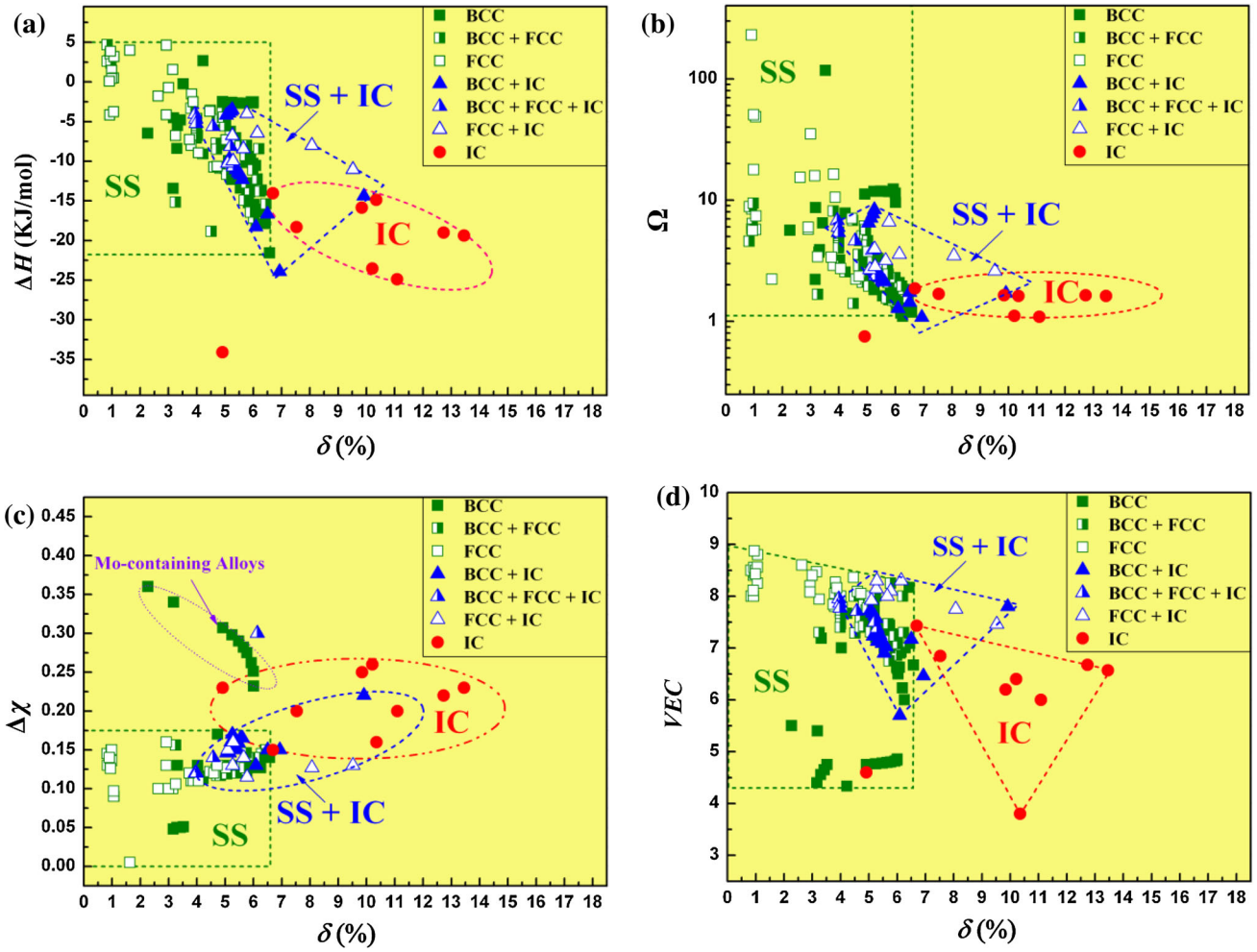

Fig. 4. The relationship between parameters δ and δH_{mix} (a), Ω (b), $\Delta\chi$ (c), and VEC (d) for previously reported multicomponent HEAs. ("SS" indicates the region where only solid solution will form for multicomponent alloys; "IC" indicates the region where the multicomponent alloys will mainly contain intermetallic compounds and other ordered phases; "S + I" indicates the region where both solid solutions ordered compounds could form).

(as shown in Table V). The calculated values of δ, ΔH_{mix}, Ω, $\Delta\chi$, and VEC for all the low-density multicomponent alloys reported in this paper are also listed in Table V. In general, intermetallic compounds also predominated in these additional alloys.

Per Table V, the relative positions of these alloys in δ versus ΔH_{mix}, δ versus Ω, δ versus $\Delta\chi$, and δ versus VEC spaces are plotted in Fig. 5. It is obvious that all have a large value of ΔH_{mix} and $\Delta\chi$ and small values of Ω and VEC. The values of δ for these alloys are in the median range: $\sim 4\% \le \delta \le 8.5\%$. Based on prior work, this is marginal to expect solid solutions, although consistent with $Al_{80}Li_5Mg_5Zn_5Sn_5$ and $Al_{80}Li_5Mg_5Zn_5Cu_5$ alloys containing predominantly α-Al phase. Nevertheless, these parameters do not serve as well as for higher density alloys. For example, as shown in Fig. 5a and b, there is considerable overlap for the regions identified with intermetallic compounds (I) and solid solutions (SS). The preference of low-density multicomponent alloys to form ordered phases more readily than traditional HEAs may be attributed to the chemical bonding character of the main group elements in these alloys. Therefore, irrespective of the fundamental mechanisms, guiding rules for the formation of solid solutions in such alloys appear to be more conservative, taking on a smaller limiting values of δ ($\delta < 4.5\%$), and larger values of ΔH_{mix} (-1 kJ/mol $< \Delta H_{mix} \le 5$ kJ/mol) and Ω ($\Omega > \sim 10$).

Of the predictive metrics evaluated (δ, ΔH_{mix}, Ω, $\Delta\chi$, and *VEC*), the electronegativity parameter, $\Delta\chi$, appears to distinguish solution-forming behavior most consistently. If the alloy possesses a sufficiently high $\Delta\chi$, highly electronegative elements will acquire electrons, the highly electropositive elements will lose electrons, and compound formation is promoted. Values for this parameter parse solid solution and intermetallic compound behavior at a critical value of about 0.175. Using this parameter alone, it is found that, except for $Al_{80}Li_5Mg_5Zn_5Sn_5$ and $Al_{80}Li_5Mg_5Zn_5Cu_5$, the investigated low-density

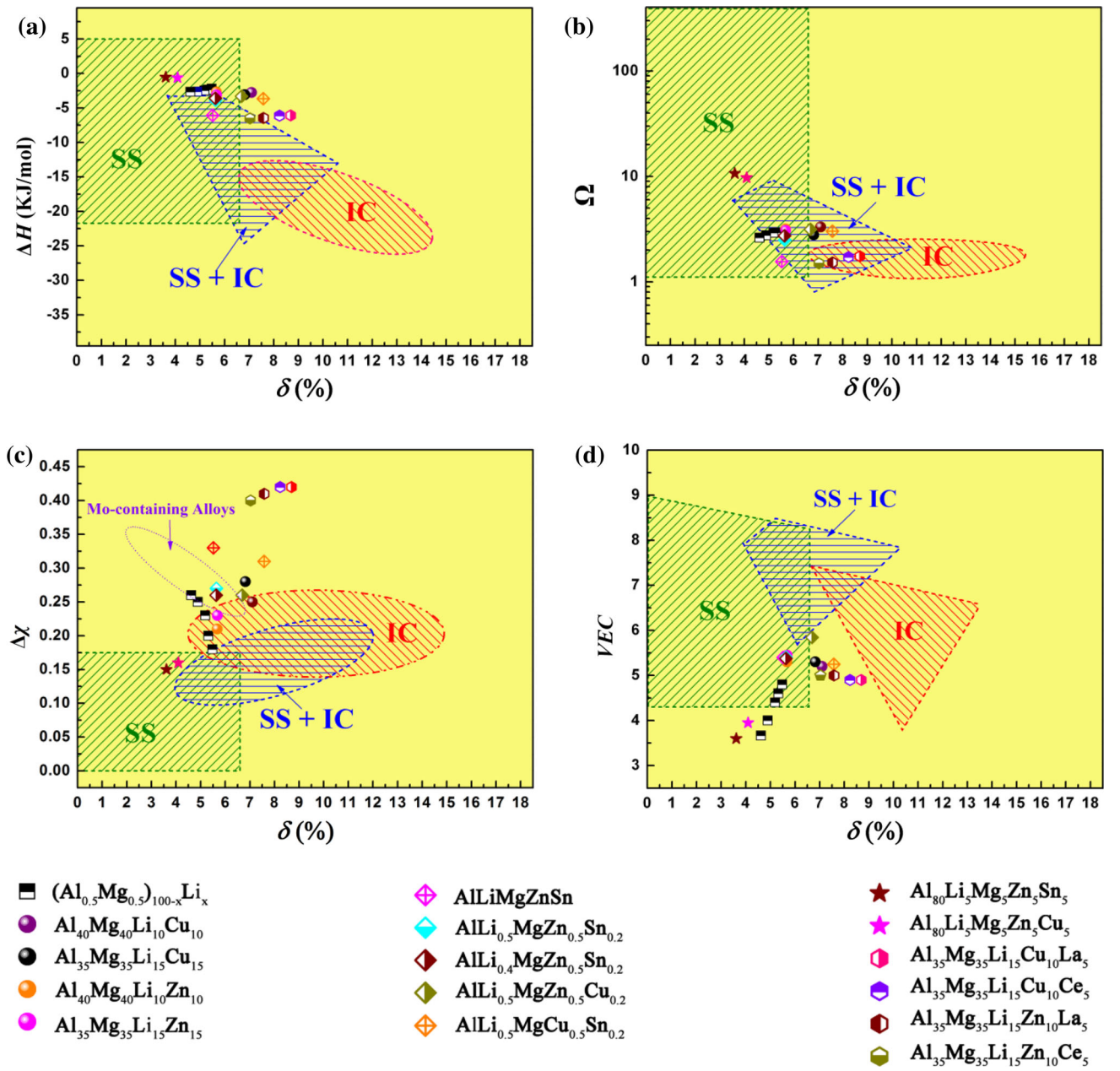

Fig. 5. Phase constituent prediction maps: (a) $\delta - \Delta H_{mix}$, (b) $\delta - \Omega$, (c) $\delta - \Delta\chi$, and (d) $\delta -$ VEC plots for multicomponent alloys in this work overlaid on cross-hatched regions developed in previous HEA investigations. (For $(Al_{0.5}Mg_{0.5})_{100-x}Li_x$, x = 5, 10, 15, 25, and 33.33).

alloys are all located outside the solid solution forming region ($\Delta\chi \geq 0.175$). The positions of the $Al_{80}Li_5Mg_5Zn_5Sn_5$ and $Al_{80}Li_5Mg_5Zn_5Cu_5$ alloys are close to the solid solution boundary, such that the formation of minor ordered phases could also be expected.

An alternative approach to predictive constitutive behavior is possible by examining the *distribution* of $\Delta\chi$ values, instead of defining a single critical value, for a selected composition. By ranking the values of $\Delta\chi$ for all alloys reported herein, the distribution of $\Delta\chi$ values as they relate to phase stability is shown in Fig. 6. This analysis illustrates that predominantly solid solution alloys possess typically low values of $\Delta\chi$, around 0.10–0.15, while (previously reported) alloys containing mostly intermetallic compounds, or mixtures of solution and compound phases, display an intermediate range of $\Delta\chi$ values, 0.15–0.25. The values of $\Delta\chi$ for the low-density alloys of the present study are positioned generally higher, 0.15–0.40, than that of previously reported alloys. Among these, $Al_{80}Li_5Mg_5Zn_5Sn_5$ and $Al_{80}Li_5Mg_5Zn_5Cu_5$ alloys have the lowest value of $\Delta\chi$, which is consistent with experiment. This trend is marked and useful.

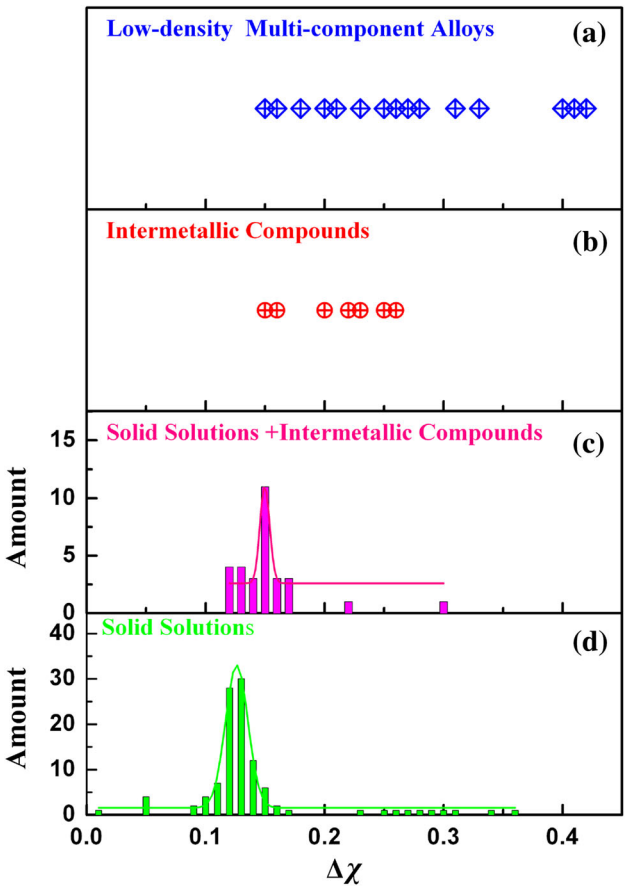

Fig. 6. Values and frequency distributions (c and d) of electronegativity difference ($\Delta\chi$) for (a) low-density multicomponent alloys (this work); (b) intermetallic phase stabilized HEAs; (c) HEAs containing both solid solution and intermetallic phases; and (d) HEAs consisting of only solid solution phases.

By analyzing phase formation rules in many different complex and rich alloys, the present results show that it is difficult to form disordered solid solutions in low-density alloys based on Al, Mg, and Li, despite configurational entropy effects. Clearly, this is a result of differences in bonding character, and perhaps due to the lack of d-orbitals in lower density elements[27] preventing higher order hybridization. It is found that although the alloys in this study exhibit low density, the competition between enthalpy and entropy is in favor of compound formation for such chemistries. Therefore, the high entropy alloy concept is likely to mainly benefit the discovery of somewhat more dense systems based on constituents of higher atomic number.

CONCLUSION

In light of the demand for lightweight structural materials for aerospace, a set of low-density quinary alloys from the Al-Li-Mg-(Zn, Cu, Sn) system was investigated. While all alloys exhibited a density well below that of common titanium alloys (4.54 g/cm^3), the microstructures of these alloys were dominated by various intermetallic compounds in the as-cast state, with the exception of $Al_{80}Li_5Mg_5Zn_5Sn_5$ and $Al_{80}Li_5Mg_5Zn_5Cu_5$, which were predominantly FCC α-Al. To better understand factors controlling phase stability in these alloys, the effects of entropy, atomic size, enthalpy effect, electronegativity, and valence electron concentration on phase formation were analyzed. The results indicate that configurational entropy is not sufficient to stabilize a majority of disordered solid solution phase in low-density alloys containing significant amounts of Al, Mg, and Li. Critical values of predictive parameters have been modified to account for the apparent difference in behavior for light element compositions, constituting a smaller value of δ ($\delta < 4.5\%$), a larger values of ΔH_{mix} (-1 kJ/mol $< \Delta H_{\text{mix}} \leq 5$ kJ/mol), and Ω ($\Omega > \sim 10$). The electronegativity parameter, $\Delta\chi$, was found to be more prognostic across the larger spectrum of high entropy alloys, where $\Delta\chi \geq 0.175$ generally indicates that intermetallic compounds are stabilized.

ACKNOWLEDGEMENTS

This research was financially supported by The Boeing Company, through Research and Development Project Agreement 2012-SDB-003.

REFERENCES

1. J.W. Yeh, S.K. Chen, S.J. Lin, J.Y. Gan, T.S. Chin, T.T. Shun, C.H. Tsau, and S.Y. Chang, *Adv. Eng. Mater.* 6, 299 (2004).
2. Y.J. Zhou, Y. Zhang, F.J. Wang, and G.L. Chen, *Appl. Phys. Lett.* 92, 241917 (2008).
3. O.N. Senkov, G.B. Wilks, J.M. Scott, and D.B. Miracle, *Intermetallics* 19, 698 (2011).
4. M.H. Chuang, M.H. Tsai, W.R. Wang, S.J. Lin, and J.W. Yeh, *Acta Mater.* 59, 6308 (2011).
5. M.A. Hemphill, T. Yuan, G.Y. Wang, J.W. Yeh, C.W. Tsai, A. Chuang, and P.K. Liaw, *Acta Mater.* 60, 5723 (2012).
6. Y. Zhang, X. Yang, and P. Liaw, *JOM* 64, 830 (2012).
7. J.W. Yeh, S.J. Lin, T.S. Chin, J.Y. Gan, S.K. Chen, T.T. Shun, C.H. Tsau, and S.Y. Chou, *Metall. Mater. Trans. A* 35, 2533 (2004).
8. C. Ng, S. Guo, J. Luan, S. Shi, and C.T. Liu, *Intermetallics* 31, 165 (2012).
9. Y. Zhang, Y.J. Zhou, J.P. Lin, G.L. Chen, and P.K. Liaw, *Adv. Eng. Mater.* 10, 534 (2008).
10. Y.J. Zhou, Y. Zhang, Y.L. Wang, and G.L. Chen, *Appl. Phys. Lett.* 90, 181904 (2007).
11. S. Singh, N. Wanderka, B.S. Murty, U. Glatzel, and J. Banhart, *Acta Mater.* 59, 182 (2011).
12. C.M. Lin and H.L. Tsai, *Intermetallics* 19, 288 (2011).
13. H. Zhang, Y. Pan, Y.Z. He, and H.S. Jiao, *Appl. Surf. Sci.* 257, 2259 (2011).
14. J.M. Zhu, H.M. Fu, H.F. Zhang, A.M. Wang, H. Li, and Z.Q. Hu, *Mater. Sci. Eng. A.* 527, 6975 (2010).
15. Y. Zhang and W.J. Peng, *Proc. Eng.* 27, 1169 (2012).
16. W.R. Wang, W.L. Wang, S.C. Wang, Y.C. Tsai, C.H. Lai, and J.W. Yeh, *Intermetallics* 26, 44 (2012).
17. O.N. Senkov and C.F. Woodward, *Mater. Sci. Eng. A* 529, 311 (2011).
18. O.N. Senkov, J.M. Scott, S.V. Senkova, D.B. Miracle, and C.F. Woodward, *J. Alloy Compd.* 509, 6043 (2011).
19. O.N. Senkov, G.B. Wilks, D.B. Miracle, C.P. Chuang, and P.K. Liaw, *Intermetallics* 18, 1758 (2010).
20. R.R. Boyer, *Mater. Sci. Eng. A* 213, 103 (1996).

21. Z. Huda, N.I. Taib, and T. Zaharinie, *Mater. Chem. Phys.* 113, 515 (2009).
22. G. Arruebarrena, I. Hurtado, J. Väinölä, C. Cingi, S. Dévényi, J. Townsend, S. Mahmood, A. Wendt, K. Weiss, and A. Ben-Dov, *Adv. Eng. Mater.* 9, 751 (2007).
23. M. Nakai and T. Eto, *Mater. Sci. Eng. A* 285, 62 (2000).
24. J.C. Williams and E.A. Starke Jr, *Acta Mater.* 51, 5775 (2003).
25. C. Kittel, *Introduction to Solid State Physics* (New York: Wiley, 1996).
26. "E;e,emts" (Wikipedia), http://en.wikipedia.org/wiki/element.
27. F. Otto, Y. Yang, H. Bei, and E.P. George, *Acta Mater.* 61, 2628 (2013).
28. MIS-Eureka Database (Stuttgart, Germany), http://www.msieureka.com.
29. S. Guo, Q. Hu, C. Ng, and C.T. Liu, *Intermetallics* 41, 96 (2013).
30. O.N. Senkov, S.V. Senkova, C. Woodward, and D.B. Miracle, *Acta Mater.* 61, 1545 (2013).
31. A.R. Miedema, P.F. de Châtel, and F.R. de Boer, *Physica B+C* 100, 1 (1980).
32. X. Yang and Y. Zhang, *Mater. Chem. Phys.* 132, 233 (2012).
33. Y. Zhang, *Mater. Sci. Forum* 654–656, 1058 (2010).
34. S. Guo and C.T. Liu, *Prog. Nat. Sci.* 21, 433 (2011).
35. S. Fang, X. Xiao, L. Xia, W. Li, Y. Dong, and , *J. Non-Cryst. Solids* 321, 120 (2003).
36. X. Yang, Y. Zhang, and P.K. Liaw, *Proc. Eng.* 36, 292 (2012).